Electronic structure and chemical bonding of the electron-poor II-V semiconductors ZnSb and ZnAs

Daryn Benson,[1,*] Otto F. Sankey,[1] and Ulrich Häussermann[2]

[1]*Department of Physics, Arizona State University, Tempe, Arizona 85287-1504, USA*
[2]*Department of Chemistry and Biochemistry, Arizona State University, Tempe, Arizona 85287-1604, USA*

The binary compounds ZnSb and ZnAs with the CdSb structure are semiconductors (II-V), although the average electron concentration (3.5 per atom) is lower than that of the tetrahedrally bonded III-V and II-VI archetype systems (four per atom). We report a detailed electronic structure and chemical bonding analysis for ZnSb and ZnAs based on first-principles calculations. ZnSb and ZnAs are compared to the zinc blende-type semiconductors GaSb, ZnTe, GaAs, and ZnSe, as well as the more ionic, hypothetical, II-V systems MgSb and MgAs. We establish a clearly covalent bonding scenario for ZnSb and ZnAs where multicenter bonded structural entities (rhomboid rings Zn_2Sb_2 and Zn_2As_2) are connected to each other by classical two-center, two-electron bonds. This bonding scenario is only compatible with a weak ionicity in II-V semiconductor systems, and weak ionicity appears as a necessary condition for the stability of the CdSb structure type. It is argued that a chemical bonding scenario with mixed multicenter and two-center bonding resembles that of boron and boron-rich compounds and is typical of electron-poor sp-bonded semiconductors with average valence electron concentrations below four per atom.

I. INTRODUCTION

Compared to the ubiquitous and technologically important III-V and II-VI systems, II-V semiconductors have received minor attention. Four equiatomic compounds are known: ZnSb, CdSb, ZnAs, and CdAs.[1,2] They all crystallize with the orthorhombic CdSb structure type. The antimonides are accessible through standard solid-state preparation techniques, whereas the arsenides require the application of high pressures. Only the properties of ZnSb and CdSb are well characterized.[3–7] Both compounds have narrow, indirect, band gaps and multivalley conduction and valence bands. This characteristic results in a high thermopower and—in conjunction with the orthorhombic symmetry—strongly anisotropic transport properties.[8,9] CdSb is an interesting material for thermoelectric sensor applications.[10–12]

With respect to the well-understood tetrahedrally bonded III-V and II-VI systems, II-V semiconductors pose some peculiarity in their bonding properties. First of all, it is not clear why the reduced electron concentration (3.5 valence electrons per atom as opposed to four) still affords semiconductor properties. Early attempts to describe CdSb by a covalent (two-center, two-electron) bonding model date back to Mooser and Pearson in 1956.[13] Later, Velicky and Frei introduced an appealing scheme where they identified an electron-deficient multicenter bonded structural unit in CdSb.[14] Alternative to a covalent bonding picture is the ionic description of II-V compound semiconductors as Zintl phases. This has been recently pursued for ZnSb and the related thermoelectric material Zn_4Sb_3.[15–17] In this case, a formal charge transfer from II to V yielding II^{2+} and V^{2-} is assumed. Now V^{2-} does not possess an electronic octet and would form a covalent bond to another V^{2-} to achieve this in the dumbbell ion V_2^{4-}. Indeed, V_2 dumbbells may be identified in the CdSb structure type.

The covalent and ionic views are rather different, and today there is no consensus. Several electronic structure studies have been performed, showing the existence of a narrow band gap and presence of complex multivalley bands.[18–21]

Most calculations referred to CdSb, whereas arsenides have not been addressed. Here, we present a detailed bonding analysis of ZnSb and ZnAs where we validate explicitly the covalent bonding picture. With a covalent (multicenter) bonding description, electron-poor II-V systems will relate to boron, which realizes semiconducting allotropes with an even lower electron concentration.

The paper is organized as follows. In Sec. II, we explain the computational procedure applied and in Sec. III crystal structure and electronic structure relationship between tetrahedrally bonded zinc blende systems and II-V ZnSb and ZnAs are worked out. Secs. IV and V are devoted to discussing chemical bonding and ionicity, respectively. Conclusions are provided in Sec. VI.

II. METHODS

Theoretical calculations of the electronic structure and total energies of cubic II-VI (II = Zn, VI = Se and Te) and III-V (III = Ga, V = As and Sb), and orthorhombic II-V (II = Zn and Mg; V = As and Sb) systems were performed by means of the first-principles all-electron projector augmented waves (PAW) method[22] as implemented in the Vienna *ab initio* Simulation Package (VASP[23]). Exchange-correlation effects were treated within the generalized gradient approximation (GGA) using the Perdew–Burke–Ernzerhof (PBE[24]) parametrization. The structures were relaxed with respect to volume, lattice parameters, and atom positions. Forces were converged to better than 1×10^{-3} eV/Å. The equilibrium volume was determined by fitting to a third-order Birch–Murnaghan[25] equation of state. The integration over the Brillouin zone (BZ) was done on a grid of special k points with size $11 \times 11 \times 11$ ($6 \times 6 \times 6$ for equation of state) determined according to the Monkhorst–Pack scheme[26] using Gaussian smearing to determine the partial occupancies for each wave function.

For calculations involving structure relaxation, the energy cutoff was set to 360 eV (Zn-V and Zn-VI), 275 eV (Mg-V, GaAs), and 225 eV (GaSb). Band structure calculations and calculations that obtained the charge densities used a high-

energy cutoff of 500 eV and the linear tetrahedron method with Blöchl[27] correction for BZ integration. Bader[28] analysis of charge densities was performed according to Ref. 29. To achieve a high accuracy for the Bader analysis the mesh for the augmentation charges was substantially increased. The error of calculated Bader charges is smaller than 0.01 e/atom.

Maximally localized Wannier functions (MLWFs) were calculated for ZnSb with the ABINIT program package using GGA-PBE as the exchange correlation and the wannier90 package as a library.[30–34] GGA-PBE pseudopotentials were provided by the ABINIT Website. These pseudopotentials are norm conserving and were generated using the fhi98PP package.[35] A $6 \times 6 \times 6$ Monkhorst–Pack k-point grid optimized for symmetry and a plane wave energy cutoff of 35 Hartree ($\sim$950 eV) was employed. The structural parameters corresponded to the relaxed structure obtained from the VASP calculations described above. MLWFs were calculated for the 68 occupied bands of the ZnSb structure. Because the Bloch orbitals are indeterminant in phase and can be degenerate in the band at distinct values of k, the Wannier functions are nonunique. For this reason, the Wannier functions

$$|\omega_n\rangle = \frac{V}{(2\pi)^3} \int_{BZ} \left[\sum_{m=1}^{N} U_{mn}^{\vec{k}} \left| \psi_{m\vec{k}} \right\rangle \right] e^{-i\vec{k}\cdot\vec{R}} d\vec{k} \qquad (1)$$

at lattice vector $\vec{R}$ are constructed from a series of unitary transformations $U_{mn}^{\vec{k}}$ of the Bloch bands $|\psi_{n\vec{k}}(\vec{r})\rangle$.[32–34] The unitary matrices $U_{mn}^{\vec{k}}$ in Eq. (1) are then chosen so that they minimize the spread Ω of the MLWFs.[32–34] The spread is defined as:

$$\Omega = \sum_{n}^{N} [\langle \omega_{n\vec{0}} | r^2 | \omega_{n\vec{0}} \rangle - \langle \omega_{n\vec{0}} | r | \omega_{n\vec{0}} \rangle^2]. \qquad (2)$$

Once the spread is iteratively minimized using conjugate gradient and steepest descent minimization routines, the resultant orbitals of Eq. (1) are the MLWFs.[33] For ZnSb, the minimum of the total spread of the MLWFs was 126.2 Å^2 with a change in spread from the previous iteration of 1.6×10^{-10} Å^2.

III. CRYSTAL STRUCTURE AND ELECTRONIC STRUCTURE RELATIONSHIPS

The III-V systems GaSb and GaAs and the II-VI systems ZnTe and ZnSe crystallize with the cubic zinc blende type (space group $F\bar{4}3m$), where all atoms are four-coordinated and connected by two-center, two-electron (2c2e) bonds [Figs. 1(a) and 1(b)]. Exchanging Ga(III) for neighboring Zn(II), or Te/Se(VI) for neighboring Sb/As(V), yields the II-V compounds ZnSb and ZnAs. These compounds crystallize with an orthorhombic $Pbca$ structure (CdSb type) which contains eight formula units in the unit cell.[1,2]

At first sight, the crystal structure of ZnSb and ZnAs also appears composed of tetrahedral entities, however, in contrast to III-V and II-VI tetrahedral frameworks, they do not exclusively share corners but also edges [Fig. 1(c)]. Edge sharing ZnV$_4$ tetrahedra imply short Zn-Zn distances. As a matter of fact, each atom in the II-V structure attains a peculiar
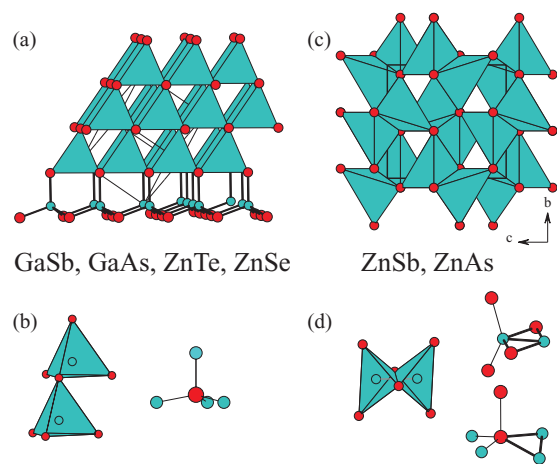

FIG. 1. (Color online) (a) Zinc blende structure as realized for GaSb, ZnTe, GaAs, and ZnSe. Polyhedra emphasize the metal atom coordination. (b) Linkage of tetrahedra in the zinc blende structure and tetrahedral coordination of atoms. (c) CdSb structure as realized for ZnSb and ZnAs. The quasitetrahedral coordination of Zn atoms by Sb/As ($=$ V) is emphasized. (d) Edge-sharing arrangement of ZnV$_4$ tetrahedra and five coordination of metal and semimetal atoms in the CdSb structure. The rhomboid ring motif Zn$_2$V$_2$ is highlighted by bold bonds. Metal atoms—cyan circles; semimetal atoms—red circles.

fivefold coordination by one like and four unlike neighbors. The nearest neighbor distances are well separated from the next nearest ones (as in the zinc blende structure). Looking closer, one recognizes that each atom is also part of planar rhomboid rings Zn$_2$V$_2$ containing the short Zn-Zn contact [Fig. 1(d)]. The arrangement of bonds and triangles (from the rhomboid ring) around each atom occurs in a tetrahedral fashion. Thus, although higher coordination numbers than four are realized, coordination is ruled by an underlying tetrahedral principle.[36]

Each rhomboid ring Zn$_2$V$_2$ is linked to 10 neighboring ones. Figure 2(a) shows a layer of rings in the ac plane. In this layer, each ring is surrounded by six neighboring ones; two are attached to the V atoms and one to the Zn atoms. This leaves one coordination site per atom to bind rings in the b direction [two up and two down per ring, Fig. 2(b)]. (Note that, because of the three axial glides, this description holds for any direction.) Table I lists the structural parameters for $F\bar{4}3m$ GaSb, GaAs, ZnTe, ZnSe, and $Pbca$ ZnSb, and ZnSb obtained from computational relaxation. These parameters are in good agreement with the experimental ones.[37] Most obvious is the volume overestimation (underbinding) by the applied GGA-PBE, which amounts to up to 4% for Zn compounds and is around 6% for Ga compounds. Including Ga 3d states in the valence shell improves this slightly (by about 0.5%). With regards to III-V and II-VI systems, our results are completely in agreement with earlier findings.[38–45]

The combination of electron count (four per atom) and tetrahedral framework ensures semiconducting properties. GaSb, GaAs, ZnTe, and ZnSe all have a direct band gaps of 0.73, 1.42, 2.39, and 2.82 eV, respectively (referring to 300 K; Ref. 46). For ZnSb and ZnAs, the electron count is lowered to 3.5. While semiconducting properties are maintained, the
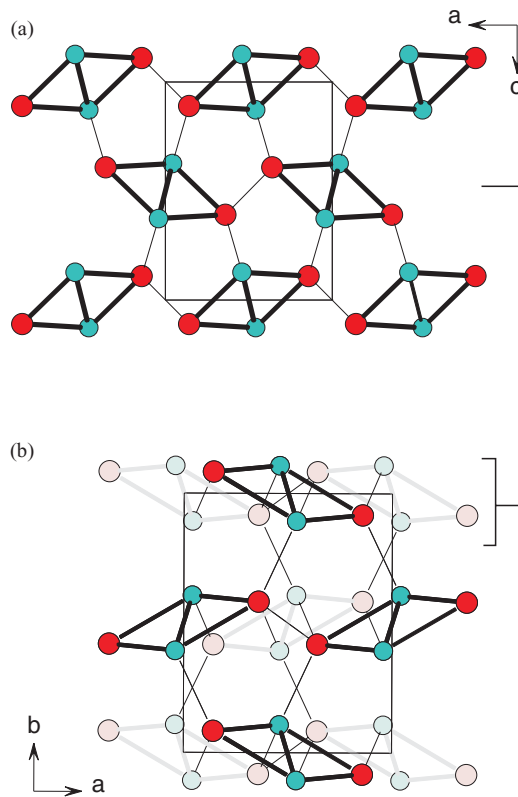
FIG. 2. (Color online) (a) Layer of connected rhomboid rings (bold bonds) in the *ab* plane of the orthorhombic CdSb structure. (b) Two layers of rhomboid rings along the *c* direction related by glide operation. The layers are distinguished by dark and pale color. Metal atoms—cyan circles; semimetal atoms—red circles.

nature of the band gap is different, and its size appears reduced. Experimentally, only the band gap of ZnSb has been determined. It has an indirect band gap of 0.5 eV.[47]

The band structures referring to the computed equilibrium structures are compiled in Fig. 3. It is well known that density functional theory gravely underestimates the size of band gaps for the tetrahedrally bonded III-V and II-VI systems.[39–45] The underbinding introduced by GGA-PBE further enhances this. For example, the calculated band gap for GaSb is zero with respect to the (underbound) theoretical equilibrium structure and about 0.6 eV for the experimental equilibrium volume. Again, this is in good agreement with previous studies.[45] The calculated band gap for orthorhombic ZnSb is 0.05 eV and thus similarly underestimated. The one for ZnAs is 0.3 eV, which suggests that the experimental band gap is probably larger than 1 eV. The increased band gap for ZnAs appears in line with the general observation that GaAs and ZnSe display larger band gaps than GaSb and ZnTe, respectively. This is

attributed to the shorter and stronger bonds formed when V or VI is from the fourth period in the periodic table.[48] The band structures of ZnSb and ZnAs are very similar to that of CdSb.[21] For all compounds, the absolute maximum of the valence band is along the Γ-X direction and local maxima are at X and Z. Likewise, the conduction band has a multivalley character. The absolute minimum is along the Γ-Z direction and local minima are along Γ-X and Γ-Y.

We note that, when going from Ga-V to Zn-V systems, the width of the valence band remains virtually the same. Also, the location and width of the V-s band relate very well for both types of systems. Zn-d bands are weakly dispersed and centered around -7 eV between the valence band and V-s bands. When comparing Zn-V with Zn-VI systems, the width of the valence band appears diminished for the latter, and the Zn-d states are centered at slightly higher energy.

IV. CHEMICAL BONDING

It is tempting to transfer the simple bonding picture for tetrahedrally bonded semiconductors to II-V systems and assign each atom in the CdSb-type framework a basis set of four sp^3 hybrid orbitals (Fig. 4). Bonds not involved in rhomboid rings are considered as 2c2e bonds. This leaves six orbitals for rhomboid ring bonding. Of the resulting molecular orbitals, two are bonding, and with four electrons occupying them, the rhomboid ring represents a four-center, four-electron (4c4e) bonded entity. Each multicenter bonded ring Zn_2V_2 (involving 4e) is connected with 2c2e bonds to 10 neighboring ones (involving 10e), and thus, equiatomic II-V systems attain an electron precise situation (electron count of 3.5 e/atom).

This appealing bonding description has been suggested earlier for CdSb[14] and ZnSb[36] but never explicitly extracted from first-principles calculations. We note that the different bonding motifs (rhomboid ring multicenter and connecting 2c2e) are well reflected in the distribution of involved interatomic distances: Zn-V interatomic distances within a ring are typically at least 0.1 Å larger than the ring connecting Zn-V distances (cf. Table II). Those in turn correlate closely with interatomic distances associated with 2e2c bonds in the corresponding III-V and II-VI systems [Ga-Sb, Zn-Te = 2.68–2.70/2.64 Å (calc/exp); Ga-As, Zn-Se = 2.49–2.50/2.45–2.46 Å (calc/exp); cf. Table I]. The peculiarly short II-II distances (2.7–2.8 Å) are a consequence of rhomboid ring multicenter bonding. The short V-V distance corresponds to a ring-linking 2c2e bond. These nearest neighbor distances associated with bonding interactions are clearly below 2.9 Å and thus well separated from the next nearest ones, starting off above 3.5 Å.

We now try to corroborate the 4c4e bonding picture by comparing and analyzing deformation charge densities. Analysis of

TABLE I. Structure parameters and band gaps of zinc blende compounds (experimental values[37] are given in parentheses).

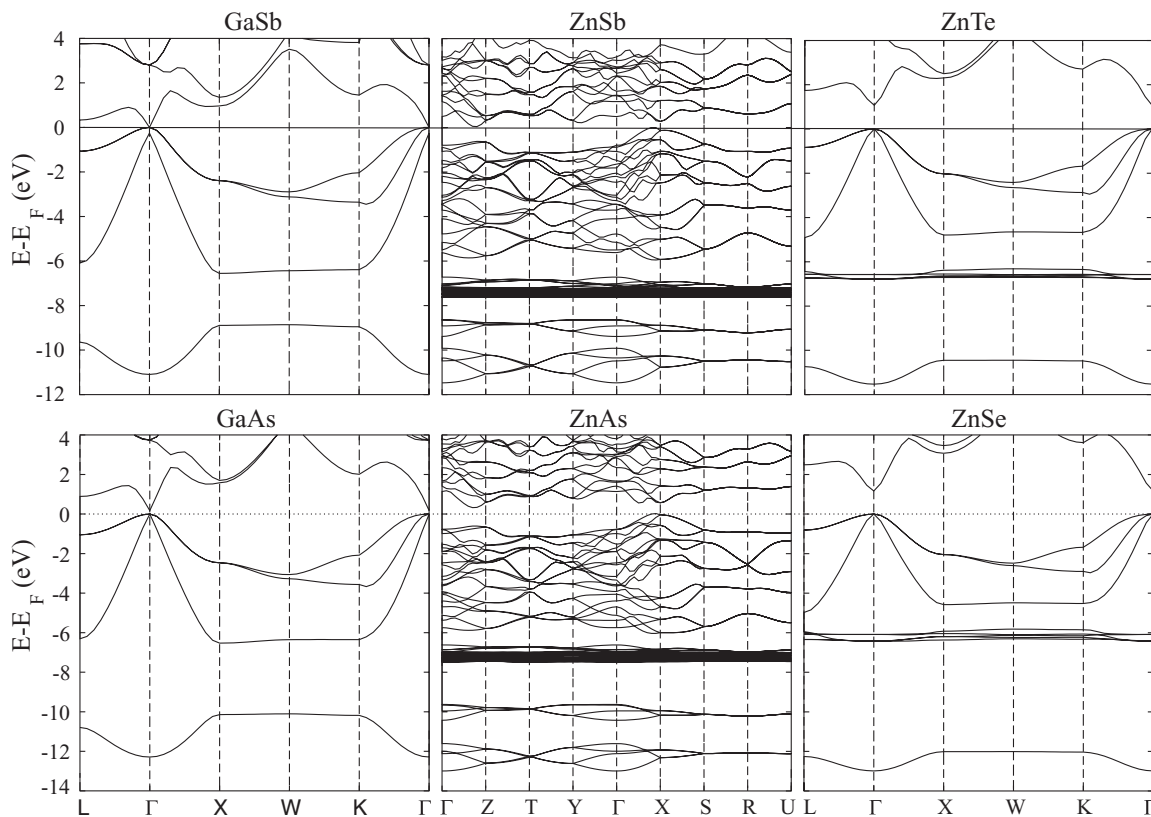| Compound	Lattice parameter (Å)	Interatomic distance (Å)	Band gap (eV)
GaSb	6.225 (6.096)	2.696 (2.637)	0 (0.75)
ZnTe	6.186 (6.103)	2.678 (2.643)	1.08 (2.39)
GaAs	5.763 (5.658)	2.496 (2.450)	0.17 (1.52)
ZnSe	5.743 (5.687)	2.487 (2.463)	1.16 (2.82)

FIG. 3. Band structures for GaSb, ZnSb, ZnTe, GaAs, ZnAs, and ZnSe at the computationally relaxed equilibrium volume. The Fermi level is indicated by a horizontal line.

charge density distributions is a classical way to extract bonding properties.[49] For obtaining deformation charge densities, $\Delta\rho$, the charge density of a superposition of non-interacting atoms is subtracted from the crystal charge density. This typically enhances the features related with bonding properties.

Figure 5 displays the situation with the tetrahedrally bonded zinc blende systems. Trivially, these archetypical systems show pronounced accumulation of charge that is associated to the 2c2e bonds. The maximum value of $\Delta\rho$ is quite precisely on the center of the interatomic line for GaSb and shifted toward the more electronegative V or VI atom in the other systems, indicating higher bond polarity. The unit cell volumes of isoelectronic systems (i.e. GaAs/ZnSe and GaSb/ZnTe) are very similar. Naturally, $\Delta\rho$ values are higher for the pair GaAs/ZnSe compared to GaSb/ZnTe because of their smaller unit cell volume. Also, within an isoelectronic pair $\Delta\rho$ values are higher for the Ga compound.

Figure 6 shows $\Delta\rho$ distributions for ZnSb and ZnAs, highlighting the rhomboid ring entity and its proposed connectivity by 2c2e bonds. The distribution associated to ring bonding is clearly different from ring-connecting bonding, the latter very similar to the $\Delta\rho$ distribution accounting for 2c2e bonding in the zinc blende systems. In particular, $\Delta\rho$ maxima for Zn-V contacts between rings appear on interatomic lines with values similar to Zn-VI contacts in the corresponding tetrahedrally bonded compounds (i.e. ZnTe for ZnSb and ZnSe for ZnAs, cf. Fig. 5). Furthermore, in terms of their $\Delta\rho$ distribution, V-V contacts are not distinguished from II-V ones, which strongly supports the picture of overall 2c2e connected rings.

Turning to rhomboid ring bonding, we note first that charge accumulation is clearly lower compared to that associated with ring-linking 2c2e bonding and second that the distribution of $\Delta\rho$ clearly suggests multicenter bonding. Intuitively, one would expect highest values for $\Delta\rho$ around the center of the
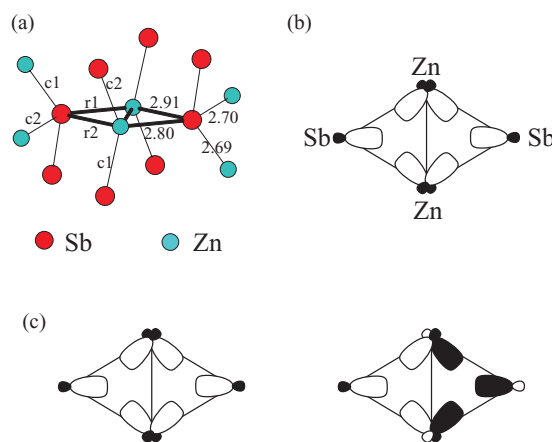

FIG. 4. (Color online) Four-center four-electron (4c4e) bond in the rhomboid ring Zn_2V_2. (a) Ring and its connecting (2c2e) bonds as in the structure of ZnSb. The two different Zn-Sb distances within the ring (r1 and r2) and connecting rings (c1 and c2) are marked. The center of a ring corresponds to a center of inversion. (b) Basis set for rhomboid ring bonding assuming sp^3 hybrid orbitals on Zn and Sb. (c) Six molecular orbitals can be constructed of which two are bonding (shown).

TABLE II. Computational structural parameters and band gaps of CdSb type II-V compounds (experimental values are given in parentheses).

Parameter	ZnSb	ZnAs	MgSb	MgAs
a (Å)	6.287 (6.202)	5.751 (5.679)	6.337	5.828
b (Å)	7.824 (7.742)	7.342 (7.277)	8.535	7.920
c (Å)	8.229 (8.100)	7.659 (7.559)	8.592	7.934
V (Å^3)	404.8 (388.9)	323.4(312.4)	4464.7	366.2
II-x	0.4598 (0.4586)	0.5395 (0.5300)	0.4670	0.5320
II-y	0.1060 (0.1128)	0.6164 (0.6140)	0.1239	0.6340
II-z	0.8731 (0.8680)	0.6337 (0.6390)	0.8577	0.6417
V-x	0.1416 (0.1420)	0.1367 (0.1410)	0.1527	0.1491
V-y	0.0830 (0.0812)	0.0739 (0.0760)	0.0734	0.0627
V-z	0.1094 (0.1077)	0.1015 (0.1000)	0.1006	0.0962
d(II-II) (Å)	2.71 (2.81)	2.71 (2.70)	3.26	3.11
d(II-V)_ r1 (Å)	2.80 (2.77)	2.61 (2.61)	2.92	2.71
d(II-V)_ r2 (Å)	2.91 (2.90)	2.72 (2.62)	2.96	2.75
d(II-V)_ c1 (Å)	2.69 (2.64)	2.50 (2.47)	2.86	2.65
d(II-V)_ c2 (Å)	2.70 (2.66)	2.53 (2.49)	2.88	2.69
d(V-V) (Å)	2.85 (2.78)	2.46 (2.46)	2.88	2.52
Band gap (eV)	0.05 (0.51)	0.30	0.92	1.11

triangles constituting the planar rhomboid rings. However, these triangles are far from equilateral; there is a shorter and longer Zn-V distance (cf. Table II). Maximum values of $\Delta\rho$ are shifted toward the triangle edge corresponding to the shorter distance. This is not an unusual phenomenon for multicenter bonded aggregates, e.g. it is also found for triangles within B_{12} icosahedra in elemental boron modifications.[50,51]
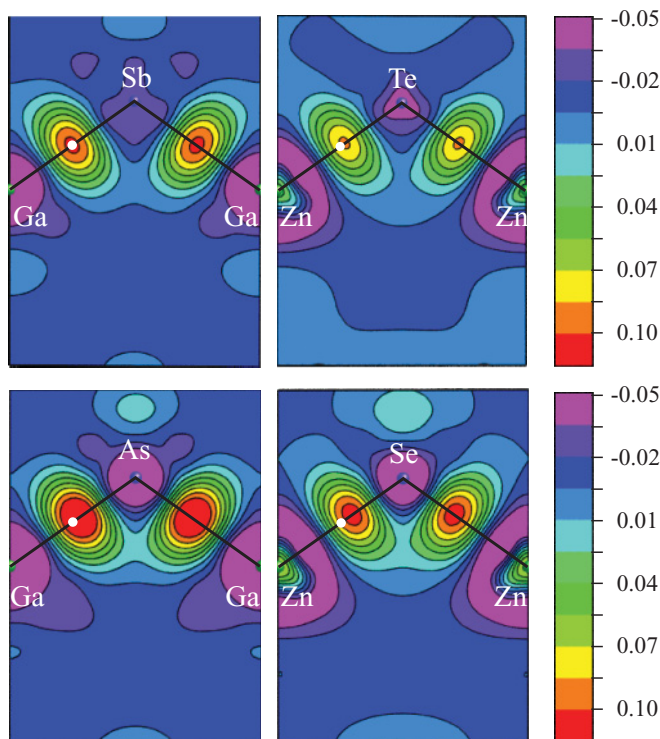

FIG. 5. (Color online) Deformation charge density distribution in GaSb, ZnTe, GaAs, and ZnSe. Contour maps are shown for the (110) plane. A color change corresponds to an isoline. The location of the center of the interatomic distance is indicated by a white circle.
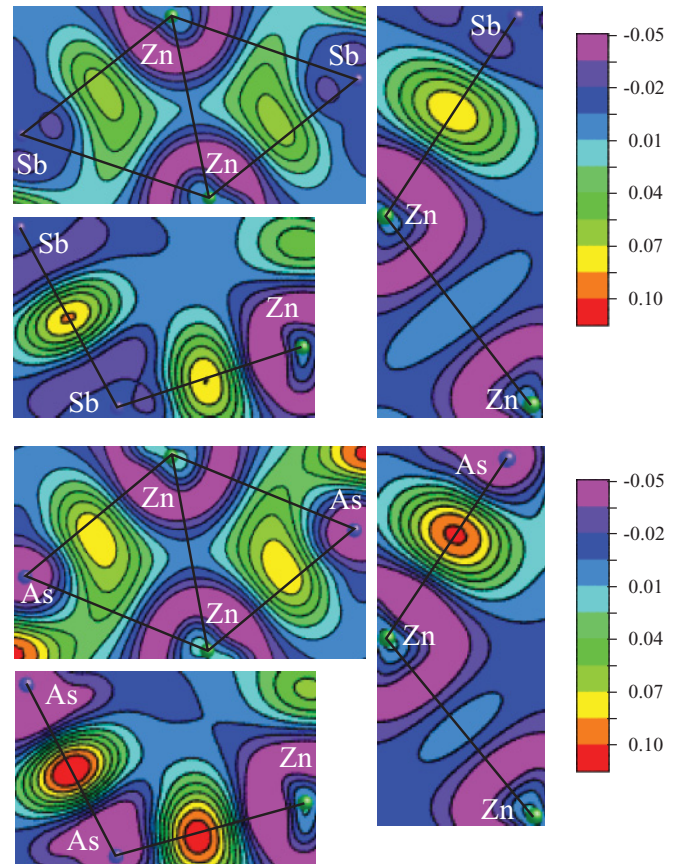

FIG. 6. (Color online) Deformation charge density distribution in ZnSb (top) and ZnAs (bottom). Contour maps are shown for the plane of the rhomboid ring and planes defined by two interatomic vectors showing ring connecting bonds. A color change corresponds to an isoline.

A strikingly similar picture is obtained from the maximally localized Wannier functions (MLWFs) in ZnSb (Fig. 7). Generally, the Wannier representation allows a real space picture of the electronic structure based on localized orbitals.[32–34] Wannier functions are constructed from extended Bloch states and are nonunique.[32–34] Marzari and Vanderbilt developed a procedure to iteratively minimize the spread of the Wannier functions so that they are well localized about their centers, hence MLWFs.[34] The MLWF calculation for ZnSb yielded 68 separated MLWFs (corresponding to the number of occupied bands), four of which corresponded to the Sb-Sb 2c2e bonds, 16 to the Zn-Sb 2c2e bonds, eight to the 4c4e bonds of the rhomboid rings, and 40 to the 5 Zn-d states on each of the eight Zn atoms within the unit cell [cf. Fig. 7(a)]. The MLWF associated with rhomboid ring bonding is clearly localized within a triangle of the ring [Fig. 7(b)]. Regions of large positive values are much closer to the more electronegative Sb atom and additionally shifted towards the triangle edge that corresponds to the shorter Zn-Sb distance. The MLWFs associated with Sb-Sb and Zn-Sb bonds are centered along the interatomic lines, which confirms their 2c2e type character [Fig. 7(b)].

In conclusion, our chemical bonding analysis for ZnSb and ZnAs strongly supports the covalent bonding picture of II-V semiconductors where multicenter (4c4e) bonded II_2V_2
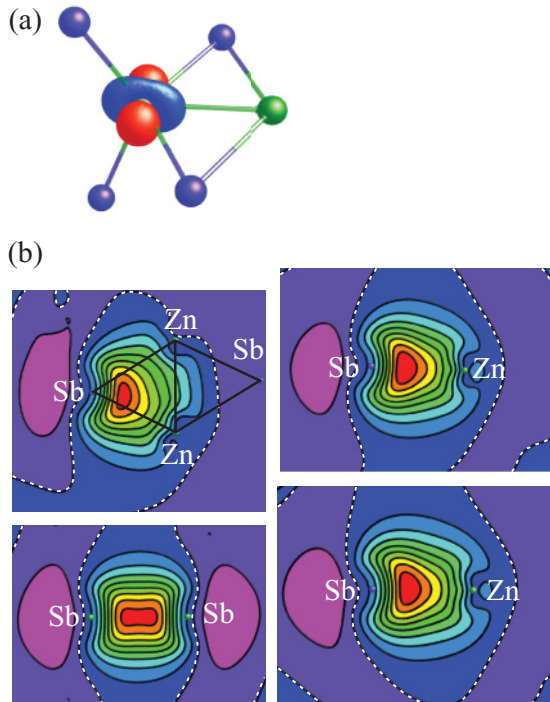
FIG. 7. (Color online) Maximally localized Wannier functions (MLWFs) in ZnSb. (a) Isosurface contour for a Zn-d type MLWF (red for positive value and blue for negative). (b) Contour maps for MLWFs associated with a rhomboid ring 4c4e bond, a 2c2e Sb-Sb bond, a c1-type 2c2e Zn-Sb bond (cf. Fig. 4(a)), and a c2-type 2c2e Zn-Sb bond (from top left counterclockwise). The broken white line separates positive from negative values.

rhomboid ring entities are linked to each other by classical 2c2e bonds.

V. IONICITY

An important issue with compound semiconductors is their ionicity. In this respect, again, the tetrahedrally bonded systems have been extensively investigated, and relations between ionicity and a wide range of physical properties were established.[52,53] In contrast with tetrahedrally bonded semiconductors, the peculiar CdSb structure occurs only with a few II-V combinations, indicating that the range of ionicity compatible with this structure is rather narrow. The border case of a large ionicity would be the earlier mentioned Zintl phase $(II^{2+})_2(V_2)^{4-}$ description of II-V semiconductors. This, however, is not supported by our bonding analysis.

To investigate ionicity in ZnSb and ZnAs, we considered the hypothetical compounds MgSb and MgAs in the CdSb structure. Among the divalent alkaline earth metals, Mg has a size closest to Zn (in terms of both metallic and ionic radius), but it is considerably more electropositive than Zn. The results of the computational structure relaxation are included in Table II. When going from ZnV to MgV, the unit cell volume increases by about 15%. However, this increase is rather anisotropic: the orthorhombic a axis is virtually unaffected, while the b axis expands by 8%. With respect to changes in interatomic distances, one notices a dramatic increase of the II-II distance within rhomboid ring entities, which suggests the
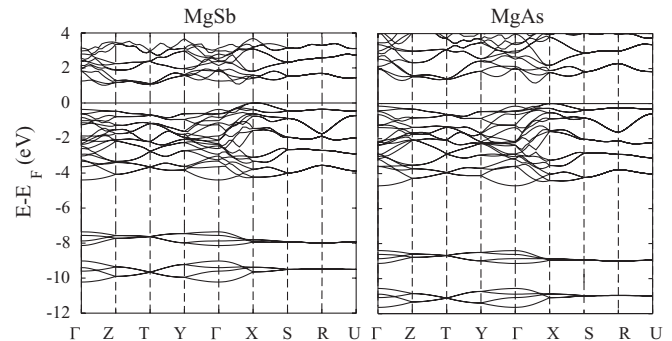

FIG. 8. Band structures for MgSb and MgAs at the computationally relaxed equilibrium volume. The horizontal line indicates a Fermi-level with states below it occupied.

loss of multicenter bonding for II = Mg. Also, II-V distances are considerably larger for II = Mg, whereas the V-V distance only slightly increases. The latter suggests the integrity of the V-V 2c2e covalent bond.

The band structures of the hypothetical compounds MgV are shown in Fig. 8. Most noticeable is their considerably larger band gap compared to ZnV systems (0.92 and 1.11 eV for MgSb and MgAs, respectively). The indirect nature of the band gap is, however, maintained. The deformation charge distributions for MgV are shown in Fig. 9. Compared to ZnV, regions of charge accumulation appear now polarized, almost ring-like, around the more electronegative V component. This is most noticeably seen in the plane of the rhomboid rings where the $\Delta\rho$ distribution is most different compared to ZnV. The $\Delta\rho$ distribution associated with Mg-V interatomic contacts is then rather associated with lone pairs around V than covalent 4c4e or 2c2e bonding as in ZnV.

In summary, the $\Delta\rho$ analysis suggests that the peculiar 4c4e bond within rhomboid rings in the CdSb structure type gets lost when ionicity is increased, and II-V semiconductors develop into Zintl phases. However, the CdSb structure seems inappropriate for accommodating an ionic Zintl phase. Compounds MgV do not exist. Instead, Mg_3V_2 with the anti-La_2O_3 structure, formally composed of Mg^{2+} and V^{3-} and no close II-II and V-V contacts, is realized. Experimental efforts to substitute partially Zn with Mg in zinc antimonides resulted in phase segregation.[54]

In an attempt to quantify ionicity, we calculated Bader charges. For this, the total charge density, including core charges, is computed. Within the PAW framework, as employed in the VASP code, the all-electron charge density $n(\vec{r})$ is obtained via a direct sum of three separate charge densities; $n(\vec{r}) = \tilde{n}(\vec{r}) + n^1(\vec{r}) - \tilde{n}^1(\vec{r})$, where $\tilde{n}(\vec{r})$ is the soft-pseudocharge density (calculated directly from the pseudowave functions on the plane-wave grid) and $n^1(\vec{r})$ and $\tilde{n}^1(\vec{r})$ are the two on site charge densities (calculated from the augmented radial grid that surrounds each ion up to a cutoff radius).[22] Nuclei represent local maxima in the charge density distribution. Atomic (Bader) regions are defined as surfaces through which the gradient of the density has zero flux.[28] By integrating the charge density within a region associated to a nucleus, the total charge on an atom can be
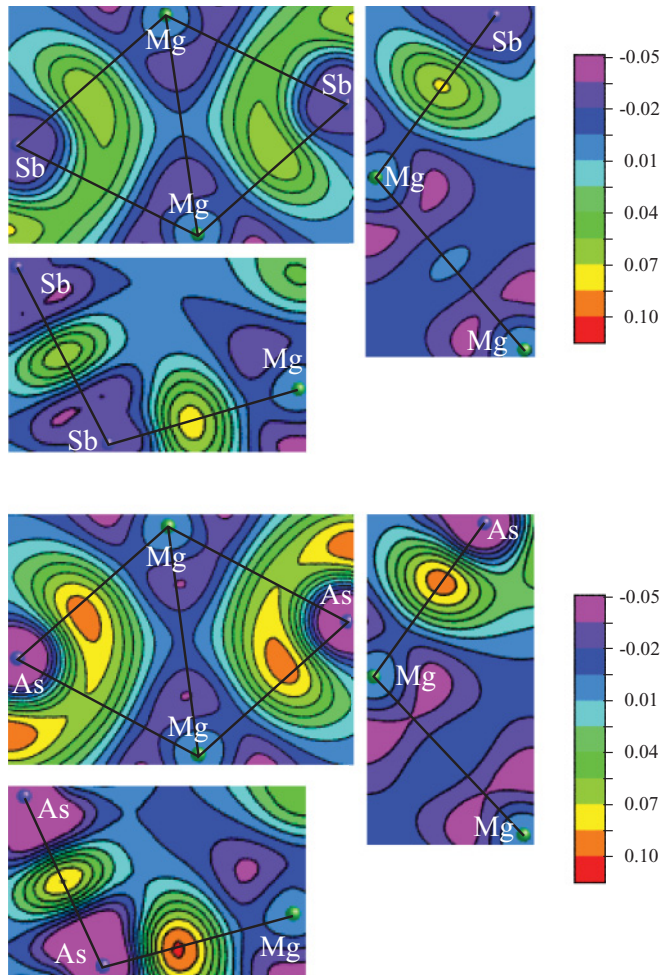
FIG. 9. (Color online) Deformation charge density distribution in MgSb (top) and MgAs (bottom). Contour maps are shown for the plane of the rhomboid ring and planes defined by two interatomic vectors showing ring connecting bonds. A color change corresponds to an isoline.

uniquely estimated.[29] Here, we compare zinc blende-type and CdSb-type compound semiconductors. Both structures consist of two Wyckoff positions for the metal and semimetal atom, respectively. Thus, in both structures, there is only one type of symmetry equivalent metal and semimetal atom, which should allow excellent comparability of obtained charges. The results are compiled in Table III. Among the tetrahedrally bonded systems, GaSb has the lowest ionicity with charges of ±0.3. For GaAs with the more electronegative As, charges increase to about ±0.6. The ionicity of the Zn-VI compounds is

TABLE III. Integrated atomic charges according to Bader.

Zinc blende structure		CdSb structure	
GaSb	±0.298	ZnSb	±0.265
GaAs	±0.615	ZnAs	±0.473
ZnTe	±1.510	MgSb	±1.415
ZnSe	±1.729	MgAs	±1.481

substantially higher compared to Ga-V systems. Now turning to Zn-V compounds, we find surprisingly low values for the Bader charges. As a matter of fact, these values are even lower than those for the corresponding Ga-V compounds, although Zn is considered more electropositive than Ga. Therefore, the analysis of Bader charges confirms our initial assumption of a low ionicity in Zn-V semiconductors. Interestingly, low ionicity for ZnSb has recently been shown also experimentally by x-ray photoelectron spectroscopy and electron energy loss measurements.[55] As expected, Bader charges for hypothetical Mg-V systems are much higher and similar to those for Zn-VI compounds.

VI. CONCLUSIONS

We have studied the electronic structure and chemical bonding of the II-V systems ZnSb and ZnAs. Both compounds are confirmed to be semiconductors with an indirect band gap and multivalley valence and conduction bands. From the analysis of deformation charge densities and maximally localized Wannier functions, we firmly establish a covalent bonding description for sp-bonded II-V semiconductors: Multicenter (4c4e) bonded rhomboid ring entities (Zn_2Sb_2 and Zn_2As_2) are connected to each other by classical two-center, two-electron bonds, and an electron-precise situation is attained for an electron count of 3.5 e/atom. This bonding model is only compatible with a low ionicty. We corroborated a low ionicty for ZnSb and ZnAs from a Bader charge analysis.

The bonding scenario for equiatomic II-V systems with mixed multicenter and two-center bonding is reminiscent of boron and boron-rich metal borides, which are the archetype of sp-bonded electron-poor semiconductors. Whereas rhomboid rings II_2V_2 are the primary structural and electronic building unit of II-V semiconductors, icosahedral clusters are those of boron. A comparison with the α-rhombohedral boron structure is most instructive. This structure consists of multicenter (skeleton) bonded icosahedra that are linked via 2c2e and 3c2e bonds to each other.[50,51] In II-V compounds, the electron count is higher, which implies that the fraction of multicenter bonding is smaller. In terms of their bonding and structural features, we may interpret the weakly ionic II-V semiconductors as a bridge between boron (with an electron count of 3 e/atom) and the tetrahedrally bonded semiconductors (with an electron count of 4 e/per atom).[56] This is also reflected in the coordination number of atoms, which is five in II-V semiconductors and, thus, intermediate between those of elemental boron structures (six or seven) and the tetrahedrally bonded II-VI and III-V systems (four), where atoms are exclusively connected by 2c2e bonds.

*daryn.benson@asu.edu

[1] K. E. Almin, Acta Chem. Scand. **2**, 400 (1948).

[2] J. Clark and K. J. Range, Z. Naturforsch. **31b**, 158 (1976).

[3] H. Komiya, K. Masumoto, and H. Y. Fan, Phys. Rev. **133**, A1679 (1964).

[4] P. J. Shaver and J. Blair, Phys. Rev. **141**, 649 (1966).

[5] E. K. Arushanov, Prog. Crystal Growth Charact. **13**, 1 (1986).

[6] F. Ermanis and E. Miller, J. Electrochemical Soc. **108**, 1048 (1961).

[7] J. Tauc and A. Abraham, Czech. J. Phys. **15**, 730 (1965).

[8] A. F. Semizorov, Inorg. Materials **34**, 770 (1998).

[9] R. Laiho, A. V. Lashkul, K. G. Lisunov, E. Lähderanta, M. O. Safonchik, and M. A. Shakhov, J. Phys. Cond. Matter **16**, 333 (2004).

[10] A. A. Snarskii, A. M. Palti, and A. A. Ashcheulov, Semiconductors **31**, 1101 (1997).

[11] A. A. Ashcheulov and I. Gutsul, J. Opt. Technol. **67**, 281 (2000).

[12] A. A. Ashcheulov, O. N. Manik, and S. F. Marenkin, Inorg. Materials **39**, S59 (2003).

[13] E. Mooser and W. B. Pearson, Phys. Rev. **101**, 1608 (1956).

[14] B. Velicky and V. Frei, Czech. J. Phys B **13**, 594 (1963).

[15] G. J. Snyder, M. Christensen, E. Nishibori, T. Caillat, and B. B. Iversen, Nat. Mater. **3**, 458 (2004).

[16] R. P. Hermann, F. Grandjean, T. C. Chen, D. E. Brown, C. E. Johnson, G. J. Snyder, and G. J. Long, Inorg. Chem. **46**, 767 (2007).

[17] S. M. Kauzlarich, S. R. Brown, and G. J. Snyder, Dalton Transaction **21**, 2099 (2007).

[18] Y. Yamada, J. Phys. Soc. Japan **35**, 1600 (1973).

[19] Y. Yamada, Phys. Stat. Solidi B **85**, 723 (1978).

[20] O. N. Manik and I. M. Rarenko, Sov. Phys. Semicond. **20**, 1068 (1986).

[21] D. M. Bercha, I. V. Slipukhina, M. Sznajder, and K. Z. Rushchanskii, Phys. Rev. B **70**, 235206 (2004).

[22] P. E. Blöchl, Phys. Rev. B **50**, 17953 (1994); G. Kresse and D. Joubert, *ibid*. **59**, 1758 (1999).

[23] G. Kresse and Hafner, J. Phys. Rev. B **48**, 13115 (1993); G. Kresse and Furthmüller, Comput. Mat. Sci **6**, 15 (1996).

[24] Y. Wang and J. P. Perdew, Phys. Rev. B **44**, 13298 (1991); J. P. Perdew, J. A. Chevary, S. H. Vosko, K. A. Jackson, M. R. Pederson, D. J. Singh, and C. Fiolhais, *ibid*. **46**, 6671 (1992).

[25] F. Birch, Phys. Rev. **71**, 809 (1947).

[26] H. J. Monkhorst and J. D. Pack, Phys. Rev. B **13**, 5188 (1976).

[27] P. E. Blöchl, O. Jepsen, and O. K. Andersen, Phys. Rev. B **49**, 16223 (1994).

[28] R. F. W. Bader, *Atoms in Molecules: A Quantum Theory* (Oxford University Press, Oxford, 1990), pp. 1–52.

[29] A. Armaldsen, W. Tang, and G. Henkelman, *Bader Charge Analysis*, [http://theory.cm.utexas.edu/bader/] (last accessed on September 14th 2011); W. Tang, E. Sanville, and G. Henkelman, J. Phys.: Condens. Matter **21**, 084204 (2009).

[30] J. P. Perdew, K. Burke, and M. Ernzerhof, Phys Rev. Let. **77**, 3865 (1996).

[31] X. Gonze, B. Amadond, P. M. Anglade, J. M. Beuken, F. Bottin, P. Boulanger, F. Bruneval, D. Caliste, R. Caracas, M. Côté, T. Deutsch, L. Genovese, Ph. Ghosez, M. Giantomassi, S. Goedecker, D. R. Hamann, P. Hermet, F. Jollet, G. Jomard, S. Leroux, M. Mancini, S. Mazevet, M. J. T. Oliveira, G. Onida, Y. Pouillon, T. Rangel, G. M. Rignanese, D. Sangalli, R. Shaltaf, M. Torrent, M. J. Verstraete, G. Zerah, and J. W. Zwanziger, Computer Phys. Comm. **180**, 2582 (2009).

[32] N. Marzari and D. Vanderbilt, Phys. Rev. B **56**, 12847 (1997).

[33] A. A. Mostofi, J. R. Yates, Y. S. Lee, I. Souza, D. Vanderbilt, and N. Marzari, Comp. Phys. Comm. **178**, 685 (2008).

[34] I. Souza, N. Marzari, and D. Vanderbilt, Phys. Rev. B **65**, 035109 (2001).

[35] M. Fuchs and M. Scheffler, Comput. Phys. Commun. **119**, 67 (1999).

[36] A. S. Mikhaylushkin, J. Nylen, and U. Häussermann, Chem. Eur. J. **11**, 4912 (2005).

[37] P. Villars and L. D. Calvert, *Pearson's Handbook of Crystallographic Data for Intermetallic Compounds* (Sec. Ed., ASM International, Ohio, 1991).

[38] S. Zh. Karazhanov, P. Ravindran, A. Kjekshus, H. Fjellvåg, and B. G. Svensson, Phys. Rev. B **75**, 155104 (2007).

[39] S. Z. Karazhanova, P. Ravindran, A. Kjekhus, H. Fjellvåg, U. Grossner, and B. G. Svensson, J. Crystal Growth **287**, 162 (2006).

[40] R. Khenata, A. Bouhemadou, M. Sahnoun, A. H. Reshak, H. Baltache, and M. Rabah, Computational Materials Science **38**, 29 (2006).

[41] J. H. Yang, S. Chen, W. J. Yin, X. G. Gong, A. Walsh, and S. H. Wei, Phys. Rev. B **79**, 245202 (2009).

[42] R. Miotto, G. P. Srivastava, and A. C. Ferraz, Phys. Rev. B **59**, 3008 (1999).

[43] B. K. Agrawal, P. S. Yadav, S. Kumar, and S. Agrawal, Phys. Rev. B **52**, 4896 (1995).

[44] S. H. Rhim, M. Kim, A. J. Freeman, and R. Asahi, Phys Rev. B **71**, 045202 (2005).

[45] R. Ahmed, F. E. Aleem, S. J. Hashemifar, H. Rashid, and H. Akbarzadeh, Commun. Theor. Phys. **52**, 527 (2009); J. M. Smith, *Molecular Dynamics* (Academic, New York, 1980), Vol. 2, p. 20.

[46] C. Kittel, *Introduction to Solid State Physics*, 6th Ed., (John Wiley, New York, 1986), p. 185; [http://www.semiconductors.co.uk/].

[47] M. Zavetova, Phys. Stat. Sol. **5**, K19 (1964).

[48] R. Sproull and W. Phillips, *Modern Physics: The Quantum Physics of Atoms, Solids and Nuclei*, 3rd ed. (John Wiley, New York, 1980), p. 309.

[49] T. S. Koritsanszky and P. Coppens, Chem. Rev. **101**, 1583 (2001).

[50] M. Fujimori, T. Nakata, T. Nakayama, E. Nishibori, K. Kimura, M. Takata, and M. Sakata, Phys. Rev. Lett. **82**, 4452 (1999).

[51] S. Hosoi, H. Kim, T. Nagata, K. Kirihara, K. Soga, K. Kimura, K. Kato, and M. Takata, J. Phys. Soc. Jpn **76**, 044602 (2007).

[52] J. C. Phillips, Rev. Mod. Phys. **42**, 317 (1970).

[53] N. E. Christensen, S. Satpathy, and Z. Pawlowska, Phys. Rev. B **36**, 1032 (1987).

[54] F. Ahmadpour, T. Kolodiazhnyi, and Y. Mozharivskyj, J. Solid State Chem. **180**, 2420 (2007).

[55] P. H. M. Böttger, S. Diplas, E. Flage-Larsen, O. Prytz, and T. G. Finstad, J. Phys. Cond. Matter **23**, 265502 (2011).

[56] U. Häussermann and A. S. Mikhaylushkin, Dalton Transaction **39**, 1036 (2010).